A LETTERS JOURNAL EXPLORING THE FRONTIERS OF PHYSICS

OFFPRINT

Anisotropic constraints on energy distribution in rotating and stratified turbulence

S. KURIEN, B. WINGATE and M. A. TAYLOR

EPL, **84** (2008) 24003

TAKE A LOOK AT THE NEW EPL

Europhysics Letters (EPL) has a new online home at
www.epljournal.org

Take a look for the latest journal news and information on:

- reading the latest articles, free!
- receiving free e-mail alerts
- submitting your work to EPL

www.epljournal.org

epl A Letters Journal Exploring the Frontiers of Physics

October 2008

EPL, **84** (2008) 24003 www.epljournal.org
doi: 10.1209/0295-5075/84/24003

Anisotropic constraints on energy distribution in rotating and stratified turbulence

S. Kurien[1(a)], B. Wingate[2] and M. A. Taylor[3]

[1] *Theoretical Division, Los Alamos National Laboratory - Los Alamos, NM 87545, USA*
[2] *Computer and Computational Sciences Division, Los Alamos National Laboratory - Los Alamos, NM 87545, USA*
[3] *Exploratory Simulations Technologies, Sandia National Laboratories - Albuquerque, NM 87185, USA*

received 27 March 2008; accepted in final form 8 September 2008
published online 8 October 2008

PACS 47.27.-i – Turbulent flows
PACS 47.32.-y – Vortex dynamics; rotating fluids
PACS 47.55.Hd – Stratified flows

Abstract – It is shown that for Boussinesq flows in which rotation and stratification are equally strong, the forward cascade of potential enstrophy constrains the spectral distribution of horizontal kinetic energy and potential energy. Horizontal kinetic energy is suppressed in the small–aspect-ratio wave modes, and potential energy in suppressed in the large–aspect-ratio wave modes. Scaling estimates based on phenomenological arguments yield scaling of k_h^{-3} and k_z^{-3}, respectively, of the two spectra. High-resolution numerical simulations of the Boussinesq equations in the relevant parameter regimes show spectral scaling exponent closer to -4, and hence even stronger suppression than is predicted by dimensional estimates.

Introduction. – It is well known that in two-dimensional (2d) turbulence the downscale transfer of energy is suppressed due to predominant downscale transfer of enstrophy, the second invariant in 2d flows [1,2]. The energy is thus forced to transfer to the larger scales, in the so-called inverse cascade. In general, it appears that if there is more than one invariant in a hydrodynamical system and they are related in wave number space, they can impose contraints on each other which determine the direction of dominant transfer of each [3].

Another classical example of such mutually constrained conserved quantities is found in quasi-geostrophic (QG) flow. The latter is an approximation for rapidly rotating, strongly stratified flows [4,5]. The zeroth-order expansion of the velocity in the rotation and stratification parameters is geostrophic, that is, the Coriolis force is balanced by the pressure gradient force, and the linear plane waves called inertia-gravity waves are eliminated to the lowest order. The dynamics is described by the evolution of potential vorticity q_{qg} [6]:

$$\frac{\partial q_{qg}}{\partial t} + \boldsymbol{u}_{0h} \cdot \nabla q_{qg} = 0, \tag{1}$$

where

$$q_{qg} = f\frac{\partial \theta}{\partial z} - N\omega_3, \tag{2}$$

where $\boldsymbol{u}_{0h}$ is the leading order (horizontal) geostrophically balanced velocity, θ is the density fluctuation scaled to have the same dimensions as velocity, $\omega_3 = (\nabla_h \times \boldsymbol{u}_h) \cdot \hat{\boldsymbol{z}}$ is the z-component of the vorticity, f and N are the Coriolis and Brunt-Väisälä (buoyancy) frequencies, respectively, of a system which is rotating and stratified in the z-direction.

Charney [6] showed that the global conservation of kinetic plus potential energy,

$$E_T = \frac{1}{2}\int (|\boldsymbol{u_0}|^2 + \theta^2)\mathrm{d}\boldsymbol{x}, \tag{3}$$

and potential enstrophy,

$$Q_{qg} = \frac{1}{2}\int |q_{qg}|^2 \mathrm{d}\boldsymbol{x}, \tag{4}$$

in inviscid three-dimensional (3d) QG flow, leads to an inverse (upscale) cascade of energy with corresponding low–wave-number energy spectrum

$$E_T(k) \propto \varepsilon^{2/3} k^{-5/3}, \tag{5}$$

and a forward (downscale) cascade of potential enstrophy with corresponding high–wave-number energy spectrum

$$E_T(k) \propto \varepsilon_Q^{2/3} k^{-3}. \tag{6}$$

Here k is the wave number and ε and ε_Q are the transfer rates of energy and potential enstrophy, respectively

(a) E-mail: skurien@lanl.gov

(see for example [7] for further discussion on the assumptions and details of Charney's work). Notably, the scaling predictions in eqs. (5), (6) are very similar to those for 2d turbulence, but arise not from two-dimensionality but from the truncated quasi-geostrophic dynamics of a 3d flow.

In theory, as the rotation and stratification of a 3d fluid become infinitely strong, the inertia-gravity waves are eliminated to lowest order, giving leading-order QG flow satisfying (1), (2). In practice, for very strong but finite rotation and stratification, the inertia-gravity waves continue to strongly influence the small-scale dynamics leading to $E_T(k) \sim k^{-\gamma}$, where $1 < \gamma < 2$ [8,9] in the high wave numbers. The underlying leading-order QG scaling of k^{-3} predicted by Charney can then only be extracted by separating the QG (or geostrophic) modes from the wave (or ageostrophic) modes by either suitably projecting the full solutions onto the QG modes [8,10–12] or by filtering out the ageostrophic inertia-gravity waves [5].

We consider rotating stratified turbulence as described by the Bousinnesq equations, retaining both the leading order QG as well as sub-leading contributions from inertia-gravity waves and other nonlinear waves. We show that in the regime of *equally* strong rotation and stratification, potential enstrophy imposes separate constraints on the horizontal kinetic energy and the potential energy. Let wave vector $\boldsymbol{k} = k_x\hat{\boldsymbol{x}} + k_y\hat{\boldsymbol{y}} + k_z\hat{\boldsymbol{z}}$, such that the horizontal component $k_h = (k_x^2 + k_y^2)^{1/2}$ and the vertical component is k_z. Then, the potential enstrophy suppresses potential energy in the modes with large aspect ratio $k_z/k_h \gg 1$. The resulting potential energy spectral scaling of k_z^{-3} is obtained simply by dimensional analysis and the assumption that the potential enstrophy flux (dissipation) governs the high–wave-number distribution of potential energy. Similarly, potential enstrophy also suppresses horizontal kinetic energy in modes with small aspect ratio $k_z/k_h \ll 1$ (or $k_h/h_z \gg 1$), with horizontal kinetic energy spectrum scaling of k_h^{-3} according to dimensional analysis. These are the first scaling estimates for the spectra of rapidly rotating and stably stratified flows away from pure QG, obtained solely using the relationship between potential enstrophy and energy as a function of wave number.

We must emphasize the most important feature of our results. Typically, numerical simulations of rotating and stratified flows are analyzed using the Craya-Herring decomposition [10,11] into wave (fast) and vortical (slow) modes, the latter also known as the potential-vorticity (PV) modes (see for example [8,12,13] and references therein). Using such a decomposition, one separates the fast wave modes from the slow PV modes and analyzes these separately with comparisons made to Charney's prediction for the QG modes. In the present work, the "decomposition" is not in wave modes, but rather in the separate behavior of horizontal kinetic energy and potential energy of the un-decomposed field, depending on the aspect ratio of wave number. In fact, our mathematical and numerical analysis may be more relevant to real physical flows which are in the rapidly rotating and strongly stratified regime, but are not strictly QG or for which doing mode decompositions may not be feasible due to sparseness or other limitations of field data.

Rapidly rotating and strongly stratified Boussinesq dynamics. – We begin with the Boussinesq equations [4] for rotating, stably stratified and incompressible flow as written in [14]:

$$\begin{aligned} \frac{D}{Dt}\boldsymbol{u} + f\hat{\boldsymbol{z}}\times\boldsymbol{u} + \nabla p + N\theta\hat{\boldsymbol{z}} &= \nu\nabla^2\boldsymbol{u} + \mathcal{F}, \\ \frac{D}{Dt}\theta - Nw &= \kappa\nabla^2\theta, \end{aligned} \tag{7}$$

$$\begin{aligned} \nabla\cdot\boldsymbol{u} &= 0, \\ \frac{D}{Dt} &= \frac{\partial}{\partial t} + \boldsymbol{u}\cdot\nabla, \end{aligned} \tag{8}$$

where $\boldsymbol{u}$ is the velocity, w is its vertical component, p is the effective pressure and $\mathcal{F}$ is an external input or force. The total density is given by

$$\rho_T(\boldsymbol{x}) = \rho_0 - bz + \rho(\boldsymbol{x}), \tag{9}$$

such that

$$|\rho| \ll |bz| \ll \rho_0, \tag{10}$$

where ρ_0 is the constant background, b is constant and larger than zero for stable stratification in the vertical z-coordinate, ρ is the density fluctuation. The density is normalized to $\theta = \rho(g/b\rho_0)^{1/2}$ which has the dimensions of velocity. The Coriolis parameter $f = 2\Omega$, where Ω is the constant rotation rate about the z-axis, the Brunt-Väisälä frequency $N = (gb/\rho_0)^{1/2}$, $\nu = \mu/\rho_0$ is the kinematic viscosity and κ is the mass diffusivity coefficient. We assume periodic or infinite boundary conditions. The relevant nondimensional parameters for this system are the Rossby number $Ro = f_{nl}/f$ and the Froude number $Fr = f_{nl}/N$, where $f_{nl} = (\epsilon_f k_f^2)^{1/3}$ is the nonlinear frequency given input rate of energy ϵ_f [12]. Thus Ro and Fr are the ratios of rotation and stratification timescales, respectively, to the nonlinear timescale.

The Boussinesq equations conserve the following quantities for $\mathcal{F} = \nu = \kappa = 0$:

$$\begin{aligned} \text{total energy } E_T = E + P, \quad \frac{D}{Dt}\int E_T \,\mathrm{d}\boldsymbol{x} &= 0, \\ \text{potential vorticity } q = \left(\boldsymbol{\omega}_a\cdot\nabla\rho_T\right), \quad \frac{Dq}{Dt} &= 0, \\ \text{potential enstrophy } Q = \frac{1}{2}q^2, \quad \frac{DQ}{Dt} = \frac{D}{Dt}\int Q \,\mathrm{d}\boldsymbol{x} &= 0. \end{aligned}$$

$E = \frac{1}{2}|\boldsymbol{u}|^2$ is the kinetic energy, $P = \frac{1}{2}\theta^2$ is the potential energy of the density fluctuations. The absolute vorticity $\boldsymbol{\omega}_a = \boldsymbol{\omega} + f\hat{\boldsymbol{z}}$ and the relative (or local) vorticity $\boldsymbol{\omega} = \nabla\times\boldsymbol{u}$. Potential vorticity may be written in terms of θ as

$$q = fN + \boldsymbol{\omega}\cdot\nabla\theta + f\frac{\partial\theta}{\partial z} - N\omega_3. \tag{11}$$

The constant part fN does not participate in the dynamics and we will therefore neglect it from now on. The linear part of (11) is precisely q_{qg} of (2). In what follows we will assume that $\nu \to 0$ and $\kappa \to 0$ such that Prandtl number $Pr = \nu/\kappa = 1$, and the force $\mathcal{F}$ is confined to the lowest modes. Thus we assume a conventional "inertial range" of turbulent scales wherein the transfer of conserved quantities dominates over both their dissipation and forcing.

In the limit $Ro \to 0$, $Fr \to 0$, the linear waves known as inertia-gravity waves are eliminated in the leading-order solution, yielding classical QG as described by (2). Equivalently, one could project out the linear solutions of eq. (7) which carry the linear potential vorticity [8,12]. Quasi-geostrophic modes are thus a subset of the full solution to the Boussinesq equations in the limit $Ro \to 0$, $Fr \to 0$, a limit which is difficult to achieve in practice.

From the nondimensional form $q = \boldsymbol{\omega} \cdot \nabla\theta + Ro^{-1}\frac{\partial \theta}{\partial z} - Fr^{-1}\omega_3$, it is observed that as $Ro \to 0$ and $Fr \to 0$, the potential vorticity q approaches q_{qg} [8,15]. In Fourier representation:

$$\tilde{q}(\boldsymbol{k}) \simeq -ifk_z\tilde{\theta} + iN\boldsymbol{k}_h \times \tilde{\boldsymbol{u}}_h = -ifk_z\tilde{\theta} + iNk_h\tilde{u}_h, \quad (12)$$

where $\tilde{\cdot}$ denotes Fourier coefficients, the total wave vector $\boldsymbol{k} = \boldsymbol{k}_h + k_z\hat{\boldsymbol{z}}$, the horizontal wave vector component has length $k_h = (k_x^2 + k_y^2)^{1/2}$, the vertical wave number is k_z and $\boldsymbol{u}_h$ is the horizontal velocity vector with magnitude $u_h = (u_x^2 + u_y^2)^{1/2}$. We assume that the vertical velocity $w = u_z \sim 0$ in the lowest order (classical QG) thus obtaining the last equality of eq. (12). We take both N and f to be very large, and $N/f = 1$, so that $Ro = Fr$. This approaches the special case $Ro \to 0$ and $Fr \to 0$ while $Ro = Fr$ which was shown rigorously to be leading-order QG in [14]. For $k > k_f$, we consider two cases.

Large–aspect-ratio modes, $\frac{k_z}{k_h} \gg 1$. These are the more vertical wave number modes corresponding loosely to flat "pancake" scales in physical space. Equation (12) reduces to $\tilde{q} \simeq -ifk_z\tilde{\theta}$, yielding:

$$Q(k_h, k_z) = \frac{1}{2}|\tilde{q}|^2 = f^2k_z^2P(k_h, k_z), \quad (13)$$

where the potential energy spectral density is $P(k_h, k_z) = \frac{1}{2}|\tilde{\theta}|^2$. Upon integrating both sides over the vertical wave number interval $[\kappa_z, \infty]$:

$$\int_{\kappa_z}^{\infty} Q(k_h, k_z)\mathrm{d}k_z = \int_{\kappa_z}^{\infty} f^2k_z^2P(k_h, k_z)\ \mathrm{d}k_z. \quad (14)$$

Then, for large κ_z, we are lead to the following constraint:

$$\int_{\kappa_z}^{\infty} Q(k_h, k_z)\mathrm{d}k_z \gg f^2\kappa_z^2\int_{\kappa_z}^{\infty} P(k_h, k_z)\,\mathrm{d}k_z. \quad (15)$$

Thus, for sufficiently high wave numbers $\kappa_z \to \infty$, the potential enstrophy Q forms the dominant forward cascade and, in order to remain finite, suppresses the potential energy P in this regime. The dimensional argument following [2] for two-dimensional turbulence assumes that in this wave number limit, the potential energy spectrum must depend only on the potential enstrophy flux rate ε_Q and the vertical wave number k_z, so that

$$P(k_h, k_z) \sim \varepsilon_Q^{2/5}k_z^{-3}. \quad (16)$$

We will comment in the conclusion section on why this assumption may not be appropriate in this case.

Small–aspect-ratio modes, $\frac{k_h}{k_z} \gg 1$. These are the wide flat wave number modes corresponding to the tall columnar scales in physical space. In this limit eq. (12) reduces to $\tilde{q} = iNk_h\tilde{u}_h$. Following the same arguments as for potential energy above, we obtain that the potential enstrophy dominates the forward cascade in the regime $k_h/k_z \gg 1$, resulting in suppression of horizontal kinetic energy in those modes, and the following scaling estimate:

$$E_h(k_h, k_z) \sim \varepsilon_Q^{2/5}k_h^{-3}, \quad (17)$$

where the horizontal kinetic energy $E_h(k_h, k_z) = \frac{1}{2}|\tilde{u}_h|^2$. In the next sections we seek to numerically verify our predictions for the energy spectra in the two limiting regimes in wave number.

Table 1: Parameters of Boussinesq calculations: n —number of grid points to a side; k_f —forcing wave number; N —Brunt-Väisälä frequency, Ro —Rossby number; Fr —Froude number; ϵ_f —rate of input of kinetic energy.

#	n	k_f	N/f	Ro	Fr	ϵ_f
1	512	4	1	0.014	0.014	0.60
2	512	4	1	0.0072	0.0072	0.60

Numerical simulations. – We compute the Boussinesq equations (7) for $N = f$ very large, using a pseudo-spectral code in a periodic cube of side $L = 1$, with wave numbers which are integer multiples of 2π. A fourth-order Runge-Kutta time integration is used and the inertia-gravity wave frequencies are resolved in our implicit scheme. Since we are interested in the small scales (high wave numbers), we use a statistically isotropic, white in time, stochastic forcing centered at $k_f = 4$ (see [16] for more details about the forcing). The viscous dissipation is modeled using a hyperviscous term $(-1)^{p+1}\nu(\nabla^2)^p\boldsymbol{u}$, where $p = 8$ in place of the normal Laplacian viscosity term $\nu\nabla^2\boldsymbol{u}$. The hyperviscosity coefficient ν is dynamically chosen based on the energy in the highest mode for both momentum and mass diffusion following [12,17], $\nu(t) = 2.5\left(\frac{E(k_m,t)}{k_m}\right)^{1/2}k_m^{2-2p}$, where k_m is the highest available wave number and $E(k_m, t)$ is the kinetic energy in that wave number. An analogous scheme is used for the diffusion of θ. The parameters of our highest resolution runs are given in table 1. We report the results from data #2 for which Ro and Fr are the smallest.

It is worthwhile to comment on the use of power $p = 8$ of the Laplacian in the dissipation term of our numerical

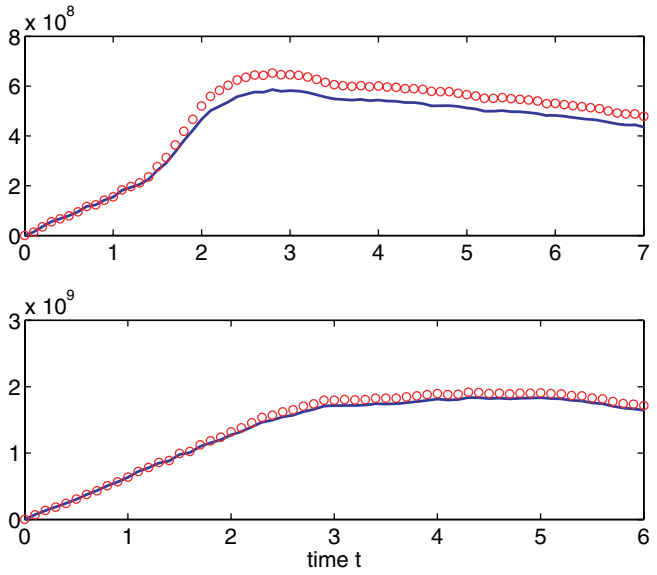

Fig. 1: Total potential enstrophy Q (line) and its quadratic part Q_{qg} (circles) for datasets 1 (top) and 2 (bottom) in table 1. As Ro and Fr decrease, the two curves become nearly indistinguishable, indicating purely quadratic potential enstrophy. Time t is in dimensional units.

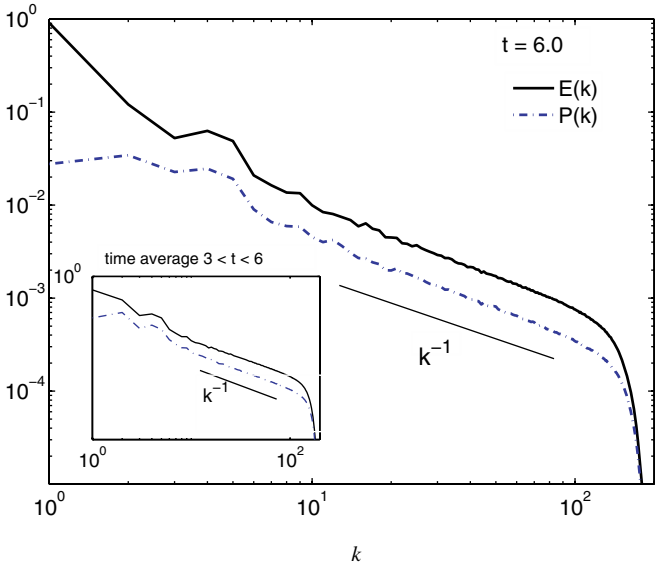

Fig. 2: Log-log plot of spherical shell averaged potential and kinetic energy spectra for data #2 at time $t = 6$. The high wave number scaling is k^{-1} indicating that in this representation the energy is dominated by waves. Inset: same spectra averaged over time $3 \leqslant t \leqslant 6$ shows that the spectra have converged over the time period that the mean potential enstrophy becomes constant (see fig. 1).

scheme. Such so-called hyperviscosity is commonly used to strongly confine dissipation to the very highest modes and hence extend the inertial range of scales. However, one must be careful that the over-damping of the small scales due to hyperviscosity does not lead to unphysical artifacts. Recently, it was shown that in eddy-damped quasi-normal Markov (EDQNM) closure simulations of three-dimensional turbulence (without rotation or stratification), that the use of a high power of the Laplacian leads to an enhanced bottleneck in the energy spectrum, to be interpreted as an incomplete thermalization [18]. Therefore, we have exerted some care in performing hyperviscous simulations. We have used the scheme of [17] which dynamically chooses the coefficient of the viscous term in order that the energy in the largest shell is resolved. There is as yet no way to pre-determine how high one can safely go in the power of the Laplacian without trial and error for a specific flow. In our case, we converged to the choice of $p = 8$ after studying lower values and noting that for this particular flow, no bottleneck appears and the inertial range is smoothly extended as the power p is increased. We also chose $p = 8$ in order to compare with the well-established simulations of Smith and Waleffe [12].

Figure 1 shows the evolution of the total potential enstrophy Q from (11) for data #1 and #2 of table 1, and its quadratic piece Q_{qg}. As Ro and Fr decrease, one observes that the total potential enstrophy becomes essentially indistinguishable from its quadratic part, indicating that the nonlinear part $\boldsymbol{\omega} \cdot \nabla\theta$ of the potential vorticity is negligible. The mean potential enstrophy has reached a nearly steady value in the time range $2.5 < t < 6$, which corresponds to between 5 and 13 nonlinear time cycles, or 5000 to 13000 rotation (stratification) cycles.

Figure 2 shows the shell-averaged kinetic and potential energy spectra for our simulation, computed as follows:

$$E(k) = \frac{1}{2}\sum_{k'} |\tilde{\boldsymbol{u}}(\boldsymbol{k}')|^2, \quad P(k) = \frac{1}{2}\sum_{k'} |\tilde{\theta}(\boldsymbol{k}')|^2,$$

where $k - 0.5 \leqslant k' < k + 0.5$ thus including all wave numbers in the spherical shell of average radius k. The scaling of both $E(k)$ and $P(k)$ is k^{-1} for $k \gg k_f$ which indicates that by this measure the high wave numbers are still dominated by waves [8,19]. The time-averaged spectra (inset) also show a scaling very close to k^{-1} indicating that the high wave numbers ($k > k_f$) have achieved close to a statistically steady state. Note that the scaling of k^{-1} for the shell-averaged spectrum is unique to the case $N/f = 1$ for small Ro and Fr [19]. In particular it is noted in [19] that if stratification dominates ($N > f$), a close to $k^{-5/3}$ spectrum is observed. This may explain the near $k^{-5/3}$ scaling observed in [13] for stratification dominated cases. Most importantly the scaling is nowhere near as steep as k^{-3} for the shell-averaged spectrum in any of these cases.

The potential energy and horizontal kinetic energy spectra as functions of k_h and k_z were computed as double sums according to

$$P(k_h, k_z) = \frac{1}{2}\sum_{k_h', k_z'} |\tilde{\theta}(\boldsymbol{k}')|^2, \qquad (18)$$

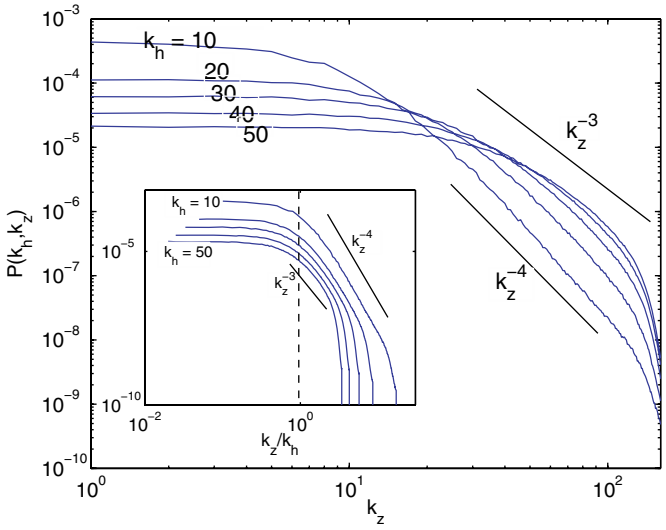

Fig. 3: Log-log plot of potential energy density $P(k_h, k_z)$ *vs.* k_z for data #2 averaged over time $3 \leqslant t \leqslant 6$. Each curve is the spectrum for a different fixed value of k_h. For $10 \leqslant k_h \leqslant 50$ and $k_z \gg k_f$, the scaling ranges between k_z^{-4} and k_z^{-3}. Inset: same spectra *vs.* k_z/k_h shows that the "turnover" to the inertial range scaling for all the curves emerges for large aspect ratio $k_z/k_h > 1$ as predicted.

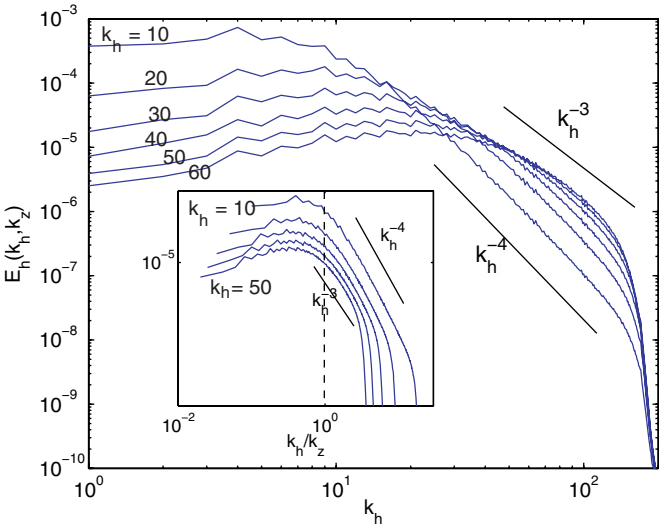

Fig. 4: Log-log plot of horizontal kinetic energy density $E_h(k_h, k_z)$ *vs.* k_h for data #2 averaged over time $3 \leqslant t \leqslant 5.2$. Each curve is a different value of k_z. For $10 \leqslant k_z \leqslant 50$ the scaling ranges between k_h^{-4} and k_h^{-3}. Inset: same spectra *vs.* k_h/k_z showing that the inertial range emerges for small aspect ratio $k_h/k_z > 1$ as predicted.

$$E_h(k_h, k_z) = \frac{1}{2} \sum_{k_h', k_z'} |\tilde{\boldsymbol{u}}_h(\boldsymbol{k}')|^2 \tag{19}$$

where $k_z[k_h] - 0.5 \leqslant k_z'[k_h'] < k_z[k_h] + 0.5$. Figure 3 shows $P(k_h, k_z)$ as a function of k_z for various values of k_h. For $10 \leqslant k_h \leqslant 50$ and $k_f \leqslant k_z \leqslant 100$, the scaling for $P(k_h, k_z)$ ranges between k_z^{-4} and k_z^{-3} indicating even stronger suppression of potential energy than the dimensional prediction of eq. (16). The inset of fig. 3 shows the same spectra *vs.* k_z/k_h; the inertial range scaling for each k_h emerges only for large aspect ratio $k_z/k_h \geqslant 1$, as predicted for eq. (16). Overall the constraints on potential energy due to potential enstrophy are dependent on wave mode aspect ratio and are highly anisotropic in scale.

Figure 4 shows $E_h(k_h, k_z)$ as a function of k_h for various values of k_z. For $10 \leqslant k_z \leqslant 50$ and $10 < k_h < 100$, the horizontal energy spectrum $E_h(k_h, k_z)$ scales between k_h^{-4} and k_h^{-3} consistent with the suppression of horizontal kinetic energy by potential enstrophy in these modes. As k_h grows, the horizontal kinetic energy persists more strongly into the high k_h. Conversely, for a fixed small k_h, the smaller k_z have more energy, indicating a growth of energy upscale in k_z. The inset of fig. 4 shows again that the inertial range scaling predicted arises only in the anisotropic small aspect ratio regime $k_h/k_z \geqslant 1$, consistent with prediction.

Conclusions. – The 512^3 resolution numerical calculations used to verify our predictions are among the highest-resolution unit aspect-ratio simulations of the Boussinesq equations performed to date. We have predicted and shown from numerical simulations, that the potential energy and horizontal kinetic energy are indeed suppressed in the large and small limits of wave number aspect ratio (k_z/k_h), respectively. Significantly, the aspect-ratio–dependent scaling exponents observed are closer to -4 (figs. 3 and 4), very different from the isotropic $k^{-\gamma}$ $(1 < \gamma < 2)$ scaling expected, for example, in the wave-dominated shell-averaged spectra (see fig. 1).

The naive expectation of -3 scaling exponent based on dimensional analysis is not observed even at these high resolutions and extreme parameter regimes. In the case of 2d turbulence, the wave number constraints between energy and enstrophy, both of which are conserved, forced the high–wave-number energy spectrum to depend only on enstrophy flux while the low–wave-number spectrum to depend only on energy flux. In the case of strongly rotating and stratified flow, the wave number constraint is between potential enstrophy (a conserved quantity) and, separately, the potential energy and horizontal kinetic energy, each of which is *not* separately conserved, as a function of aspect ratio of the wave mode. It is therefore perhaps not physically justifiable to assume that only potential enstrophy flux matters in the forward cascade. Indeed there may be some mixed dependence on both potential enstrophy as well as energy flux in both high– and low–wave-number regimes. This issue deserves further investigation.

Our main assumption in this study is that when rotation and stratification are (equally) strong, the potential vorticity becomes nearly linear, and hence the potential enstrophy nearly quadratic. We do not invoke wave mode decompositions, nor do we need to limit ourselves to only leading-order modes. In future work we will extend our

analysis to the case of $N/f \neq 1$, that is, the strength of rotation and stratification are large but unequal. The possibilities for generalized quasi-geostrophic flow [20] in which domain aspect ratio is an additional parameter, are promising areas for future research. The extension of this work to the case of low–aspect-ratio physical domains, could provide more insight into geophysical systems such as atmospheric flows. Since we do not use mode decomposition, our work may provide some connection with *in situ* or experimental data which typically cannot be mode-decomposed because of the sparseness of the one- or two-dimensional data, in contrast to numerical simulations where fully three-dimensional field data is available.

* * *

We thank G. Eyink, J. Herring, L. Smith and J. Sukhatme for valuable discussions during the course of this work. The work was funded by DOE Office of Science Advanced Scientific Computing Research (ASCR) Program in Applied Mathematics Research, the National Nuclear Security Administration of the U.S. Department of Energy at Los Alamos National Laboratory under Contract No. DE-AC52-06NA25396, the Laboratory Directed Research and Development program. Support of NSF-DMS-0529596 is also acknowledged.

REFERENCES

[1] Fjortoft R., *Tellus*, **5** (1953) 225.
[2] Kraichnan R., *Phys. Fluids*, **10** (1967) 1417.
[3] Turner L., *J. Phys. A: Math. Gen.*, **36** (2003) L481.
[4] Pedlosky J., *Geophysical Fluid Dynamics* (Springer-Verlag, New York, NY, USA) 1986.
[5] Salmon R., *Lectures on Geophysical Fluid Dynamics* (Oxford University Press, New York, NY, USA) 1998.
[6] Charney J., *J. Atmos. Sci.*, **28** (1971) 1087.
[7] Tung K. K. and Welch W. T., *J. Atmos. Sci.*, **58** (2001) 2009.
[8] Bartello P., *J. Atmos. Sci.*, **52** (1995) 4410.
[9] Babin A., Mahalov A., Nicolaenko B. and Zhou Y., *Theor. Comput. Fluid Dyn.*, **9** (1997) 223.
[10] Craya A., *Publ. Sci. Tech. Minist. Air* **345** (1958).
[11] Herring J., *Phys. Fluids*, **17** (1974) 859.
[12] Smith L. and Waleffe F., *J. Fluid Mech.*, **451** (2002) 145.
[13] Waite M. and Bartello P., *J. Fluid Mech.*, **568** (2006) 89.
[14] Embid P. and Majda A., *Geophys. Astrophys. Fluid Dyn.*, **87** (1998) 1.
[15] Kurien S., Smith L. and Wingate B., *J. Fluid Mech.*, **555** (2006) 131.
[16] Taylor M., Kurien S. and Eyink G., *Phys. Rev. E*, **68** (2003) 026310.
[17] Chasnov J. R., *Phys. Fluids*, **6** (1994) 1036 .
[18] Frisch U., Kurien S., Pandit R., Pauls W., Ray S., Wirth A. and Zhu J.-Z., to be published in *Phys. Rev. Lett.* (2008).
[19] Sukhatme J. and Smith L., *Phys. Fluids* **19** (2007).
[20] Julien K., Knobloch E., Milliff R. and Werne J., *J. Fluid Mech.*, **555** (2006) 233.